Geophysical Prospecting, 2003, **51**, 347–364

Phase behaviour of P-SV converted waves recorded at the sea-bed

Hengchang Dai*

British Geological Survey, Murchison House, West Mains Road, Edinburgh EH9 3LA, UK

Received November 2001, revision accepted February 2003

ABSTRACT

Shear waves recorded at or near the sea-bed, i.e. a water–sediment interface, may suffer from unwanted phase change, which is detrimental to velocity analysis and processing and degrades the quality of the final stacked or migrated image. In this study, this phenomenon is analysed for P-SV converted waves recorded at the sea-bed. Theoretical analysis shows that phase change does not occur if the converted shear waves always maintain raypaths that lie within the critical angle, provided the subsurface layering is horizontal. A phase change that is asymmetric with offset can readily be explained as being due to dipping layers at targets or the dipping sea-bed. This analysis is extended to multiple layers and anisotropic media and shows that the same conclusions hold. The analysis performed on two sets of ocean-bottom-cable seismic data shows that the majority of observations show little evidence of phase change, and occasionally display the asymmetric phase change with offset. This finding underlines the robustness of converted shear waves for imaging the horizontal subsurfaces and sea-bed as all of the offset information may be used.

INTRODUCTION

Recently, 4-C ocean-bottom-cable (OBC) seismic data have come into common use for a variety of applications. One of them is to use the P-SV converted wave to image the internal structure of a reservoir, such as the structure beneath a shallow gas cloud. An example of this is the Valhall field chalk reservoir. It is difficult to image its crest with conventional P-wave data because shallow gas attenuates the compressional energy and distorts the P-wave velocities (Thomsen *et al*. 1997; Dai, Li and Mueller 2000). S-waves, however, are not affected by the compressibility of pore fluids and thus offer the potential of generating a useful seismic image. However, understanding how the behaviour of the recorded S-wavefield relates to specific reservoir applications is a challenging task for the exploration industry.

S-waves have been used in seismic exploration for several decades. It is known that analysis of directly generated S-waves in land surface recordings is hampered by amplitude and phase changes at a range of offsets. The effect is due to the waves honouring the boundary conditions associated with the free surface, and has been fully discussed by Nuttli (1961) and Evans (1984). The offset range outside which the distortion is significant has often been called the S-wave window (Booth and Crampin 1985) to signify this offset restriction for anisotropy analysis and processing. In general, this distortion can be detrimental to velocity analyses and can degrade the quality of the final stacked or migrated image. In addition, it has implications for future work on fracture description utilizing S-wave anisotropy (Li, Kuhnel and MacBeth 1996). With the advent of widespread commercial surveying using sea-bed sensors, it is now appropriate to consider how the S-wave window concept may translate to the water–sediment interface. This is of particular relevance in the light of sea-bed surveys demonstrating enhanced imaging potential when

*E-mail: hcd@bgs.ac.uk

using S-waves to image through gas clouds (Berg, Svenning and Martin 1994; Thomsen *et al*. 1997). Such findings also have serious implications for AVO (Mazzotti 1991) and future time-lapse studies.

Recent work by MacBeth (1997, 1998) has demonstrated that S-wave recording at, or near, the sea-bed may indeed suffer from a similar problem. This study considered the case of plane waves incident upon the water–solid interface from a conversion point at depth. The impact of the distortion was assessed using analytic calculations together with a synthetic seismogram study. The general conclusion, based on models simulating several different sediment conditions, was that significant discrepancies could in fact arise both in the geophone recordings and in the hydrophone pressure recordings. The effect could potentially compound difficulties that are already experienced with coupling, the choice of sensor package and deployment method. In this work, these conclusions are developed further by examining the offset-dependent phase estimates for these field data sets acquired in different geographical areas.

THEORY

The P-SV converted wave of OBC seismic data discussed here is a P-wave generated from a source located at sea-surface level, converted to an SV-wave on reflection at depth and returned to a receiver located at the sea-bed, i.e. a water–solid interface. Its amplitude and phase behaviour are determined by the raypath and the velocity–depth structure of the sea-bed. To understand this, we analyse the amplitude and phase behaviour of the plane body waves incident at the water–solid interface, and the behaviour of the upgoing SV-waves converted from a deep reflector. This analysis is also applied to the case of waves propagating in vertical transverse isotropic (TIV) media.

PLANE BODY WAVES INCIDENT UPON THE WATER–SEDIMENT INTERFACE

The sea-bed can be considered as a water–solid interface. If a plane body (P- or SV-) wave is incident on this interface from below, it will generate a transmitted P-wave in the water and a reflected P-wave and an SV-wave in the solid (Fig. 1). An SH-wave generates only a reflected SH-wave in the solid. The relationship between the angles of their propagation directions is given by Snell's law:

$$\frac{\sin\theta_p}{\alpha} = \frac{\sin\theta_w}{\alpha_w} = \frac{\sin\theta_s}{\beta},$$

where α is the P-wave velocity of the solid medium, α_w is the P-wave velocity of the water, β is the S-wave velocity of the solid medium, θ_p is the angle between the P-wave raypath and the normal to the interface, θ_s is the angle between the S-wave raypath and the normal to the interface, and θ_w is the angle between the P-wave raypath in the water and the normal to the interface. Frequently, $\alpha > \alpha_w > \beta$ and we assume that this relationship holds throughout the following analysis. The phase behaviour of velocity fields recorded at such an interface has been analysed by MacBeth (1997) and in the Appendix. Here the phase behaviour of the different waves is discussed.

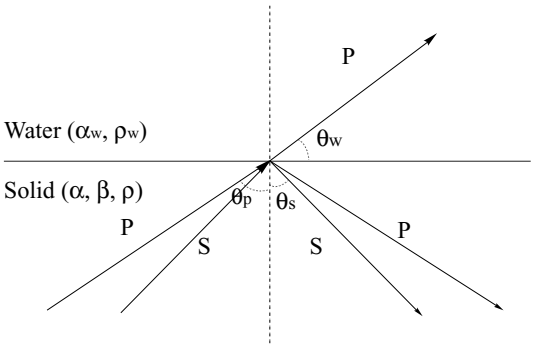

Figure 1 Plane body waves incident upon a water–isotropic solid interface.

INCIDENT P-WAVE

For an incident P-wave, the total velocity field recorded at the interface can be written as (see Appendix)

$$v_x^{\mathrm{p}}(0) = \frac{\sin 2\theta \left[\dfrac{\rho_{\mathrm{w}}}{\rho} + 2\left(\dfrac{\beta}{\alpha}\right)^2 \sqrt{\left(\dfrac{\alpha}{\beta}\right)^2 - \sin^2\theta}\sqrt{\left(\dfrac{\alpha}{\alpha_{\mathrm{w}}}\right)^2 - \sin^2\theta} \right]}{\left[\left[1 - \left(\dfrac{2\beta \sin\theta}{\alpha}\right)^2 \right] \sqrt{\left(\dfrac{\alpha}{\alpha_{\mathrm{w}}}\right)^2 - \sin^2\theta} + \dfrac{\rho_{\mathrm{w}}}{\rho}\cos\theta \right.} \\ \left. + \left(\dfrac{2\beta}{\alpha}\sin\theta\right)^2 \sqrt{\left(\dfrac{\alpha}{\alpha_{\mathrm{w}}}\right)^2 - \sin^2\theta} \left[\sin^2\theta + \cos\theta \sqrt{\left(\dfrac{\alpha}{\beta}\right)^2 - \sin^2\theta} \right] \right] = A_x(\theta) \mathrm{e}^{\mathrm{i}\phi_x(\theta)}$$

and

$$v_z^{\mathrm{p}}(0) = \frac{2\cos\theta \sqrt{\left(\dfrac{\alpha}{\alpha_{\mathrm{w}}}\right)^2 - \sin^2\theta} \left[1 - 2\left(\dfrac{\beta \sin\theta}{\alpha}\right)^2 \right]}{\left[\left[1 - \left(\dfrac{2\beta \sin\theta}{\alpha}\right)^2 \right] \sqrt{\left(\dfrac{\alpha}{\alpha_{\mathrm{w}}}\right)^2 - \sin^2\theta} + \dfrac{\rho_{\mathrm{w}}}{\rho}\cos\theta \right.} \\ \left. + \left(\dfrac{2\beta}{\alpha}\sin\theta\right)^2 \sqrt{\left(\dfrac{\alpha}{\alpha_{\mathrm{w}}}\right)^2 - \sin^2\theta} \left[\sin^2\theta + \cos\theta \sqrt{\left(\dfrac{\alpha}{\beta}\right)^2 - \sin^2\theta} \right] \right] = A_z(\theta) \mathrm{e}^{\mathrm{i}\phi_z(\theta)},$$

where θ is the angle of incidence. $v_x^{\mathrm{p}}(0)$ and $v_z^{\mathrm{p}}(0)$ are complex functions which can be decomposed into the amplitude function $A_x\,(\theta)$ and $A_z\,(\theta)$ and the phase functions $\phi_x(\theta)$ and $\phi_z(\theta)$, which indicate the phase behaviours. For the P-wave, because $\frac{\alpha}{\beta} > 1$ and $\frac{\alpha}{\alpha_{\mathrm{w}}} > 1$, all the square roots are real, and $\phi_x = \phi_z = 0$. There is no phase change at all.

INCIDENT SV-WAVE

For an incident SV-wave, the total velocity field recorded at the interface can be written as (see Appendix)

$$v_x^{\mathrm{s}}(0) = \frac{2\cos\theta \left[\cos 2\theta \sqrt{\left(\dfrac{\beta}{\alpha_{\mathrm{w}}}\right)^2 - \sin^2\theta} + \dfrac{\rho_{\mathrm{w}}}{\rho} \sqrt{\left(\dfrac{\beta}{\alpha}\right)^2 - \sin^2\theta} \right]}{\left[\cos^2 2\theta \sqrt{\left(\dfrac{\beta}{\alpha_{\mathrm{w}}}\right)^2 - \sin^2\theta} + \dfrac{\rho_{\mathrm{w}}}{\rho} \sqrt{\left(\dfrac{\beta}{\alpha}\right)^2 - \sin^2\theta} \right.} \\ \left. + 4\sin^2\theta\cos\theta \sqrt{\left(\dfrac{\beta}{\alpha_{\mathrm{w}}}\right)^2 - \sin^2\theta} \sqrt{\left(\dfrac{\beta}{\alpha}\right)^2 - \sin^2\theta} \right] = B_x(\theta) \mathrm{e}^{\mathrm{i}\phi_x(\theta)}$$

and

$$v_z^{\mathrm{s}}(0) = \frac{-4\sin\theta\cos\theta \sqrt{\left(\dfrac{\beta}{\alpha}\right)^2 - \sin^2\theta} \sqrt{\left(\dfrac{\beta}{\alpha_{\mathrm{w}}}\right)^2 - \sin^2\theta}}{\left[\cos^2 2\theta \sqrt{\left(\dfrac{\beta}{\alpha_{\mathrm{w}}}\right)^2 - \sin^2\theta} + \dfrac{\rho_{\mathrm{w}}}{\rho} \sqrt{\left(\dfrac{\beta}{\alpha}\right)^2 - \sin^2\theta} \right.} \\ \left. + 4\sin^2\theta\cos\theta \sqrt{\left(\dfrac{\beta}{\alpha_{\mathrm{w}}}\right)^2 - \sin^2\theta} \sqrt{\left(\dfrac{\beta}{\alpha}\right)^2 - \sin^2\theta} \right] = B_z(\theta) \mathrm{e}^{\mathrm{i}\phi_z(\theta)}.$$

Two critical angles exist: $\theta_1 = \arcsin(\frac{\beta}{\alpha})$ and $\theta_2 = \arcsin(\frac{\beta}{\alpha_w})$. θ_1 is always less than θ_2 because α is always larger than α_w. When the angle of incidence exceeds the smaller of the two critical angles, the square roots become imaginary and there is a phase change. In summary, the phase changes for the SV-wave are:
If $\theta \le \theta_1 = \arcsin(\frac{\beta}{\alpha})$, then $\phi_x = \phi_z = 0$.
If $\theta_1 = \arcsin(\frac{\beta}{\alpha}) \le \theta \le \theta_2 = \arcsin(\frac{\beta}{\alpha_w})$, then $\phi_x = \phi - \varphi$ and $\phi_z = \phi$, where

$$\phi = \arctan \frac{\cos^2 2\theta \sqrt{\left(\frac{\beta}{\alpha_w}\right)^2 - \sin^2\theta}}{\sqrt{\sin^2\theta - \left(\frac{\beta}{\alpha}\right)^2}\left(\frac{\rho_w}{\rho} + 4\sin^2\theta\cos\theta\sqrt{\left(\frac{\beta}{\alpha_w}\right)^2 - \sin^2\theta}\right)}$$

and

$$\varphi = \arctan \frac{\cos^2 2\theta \sqrt{\left(\frac{\beta}{\alpha_w}\right)^2 - \sin^2\theta}}{\frac{\rho_w}{\rho}\sqrt{\sin^2\theta - \left(\frac{\beta}{\alpha}\right)^2}}.$$

If $\theta_1 = \arcsin(\frac{\beta}{\alpha}) \le \theta_2 = \arcsin(\frac{\beta}{\alpha_w}) \le \theta$, then $\phi_x = \phi$ and $\phi_z = \phi - \frac{\pi}{2}$, where

$$\phi = \arctan \frac{2\sin 2\theta \sin\theta \sqrt{\sin^2\theta - \left(\frac{\beta}{\alpha_w}\right)^2}\sqrt{\sin^2\theta - \left(\frac{\beta}{\alpha}\right)^2}}{\cos^2 2\theta \sqrt{\sin^2\theta - \left(\frac{\beta}{\alpha_w}\right)^2} + \frac{\rho_w}{\rho}\sqrt{\sin^2\theta - \left(\frac{\beta}{\alpha}\right)^2}}.$$

Because the SV-wave is normally recorded only on the radial component and the P-wave only on the vertical component, the phase change is observed only on the radial component. This is highlighted in Fig. 2, where the radial component of the SV-wave recording may be seen to be constant up to a critical angle, whereupon there is a sudden phase change, followed by another, and then a subsequent smooth variation. The critical angle $\theta_1 = \arcsin(\frac{\beta}{\alpha})$ at which the phase first begins to rotate defines the edge of the S-wave window. Indeed, such phase changes are an inevitable consequence of this type of recording. To make matters worse, the cone of angles marking the critical onset may in fact be quite narrow (for example, $\theta_1 = 6.4^o$ and $\theta_2 = 7.6^o$ for $\alpha_w = 1500$ m/s, $\alpha = 1800$ m/s and $\beta = 200$ m/s). Although the theory predicts that sea-floor recordings will show a phase

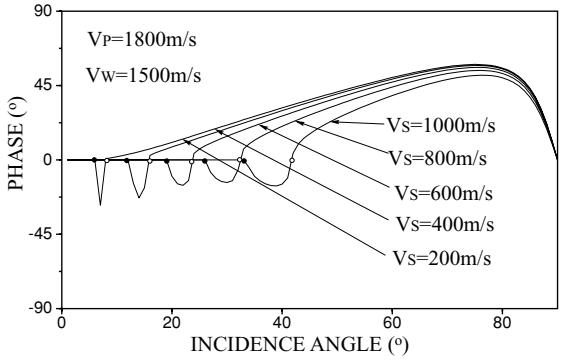

Figure 2 Phase variation of the radial component of the SV-wave recording with increasing angle of incidence. Note the abrupt transition at the critical angles related to the sediment (θ_1, black dot) and then the water layer (θ_2, white circle).

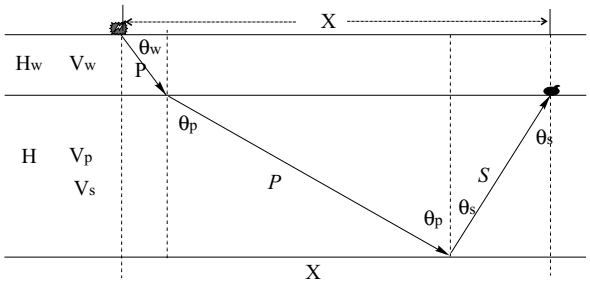

Figure 3 The P-SV converted wave raypath converted at a horizontal reflector.

change for SV energy arriving outside the shear-wave window, in reality this may not occur. This is because in OBC data we are concerned with P-SV mode-conversion where the P-wave leg has a controlling influence on the emergent SV raypath.

PHASE CHANGE OF P-SV CONVERTED WAVES CONVERTED AT A HORIZONTAL REFLECTOR

From the above discussion, we know that phase change occurs for incident SV-waves when the angle of incidence exceeds the critical angles. However, due to the effect of the water–sediment S-wave refraction, not all angles of incidence are available for the P-SV converted wave. Here, the case of a P-SV wave converted at a horizontal reflector is discussed. Figure 3 shows the acquisition geometry and the P-SV converted wave raypath. For an isotropic, horizontally layered subsurface, the horizontal slowness is constant along the raypath. Thus the take-off angle θ_w at the source is related to the propagation angle through the sea-bed sediments, θ_p, and the angle of incidence at the sea-bed receiver, θ_s. This relationship is given by Snell's law:

$$\frac{\sin\theta_p}{\alpha} = \frac{\sin\theta_w}{\alpha_w} = \frac{\sin\theta_s}{\beta}.$$

As a consequence, for any given offset, the angle of incidence at the receiver is

$$\theta_s = \arcsin\left(\frac{\beta}{\alpha}\sin\theta_p\right) = \arcsin\left(\frac{\beta}{\alpha_w}\sin\theta_w\right).$$

Clearly, θ_s is always smaller than (or at most, equal to) the critical angles $\arcsin(\frac{\beta}{\alpha})$ and $\arcsin(\frac{\beta}{\alpha_w})$ for which the S-wave window is defined between zero and $\arcsin(\frac{\beta}{\alpha})$. Indeed the limitation of θ_s is actually the critical angle $\arcsin(\frac{\beta}{\alpha})$. The relationship between the offset and angle of incidence for the geometry referred to in Fig. 3 can be written as

$$X = \frac{H\sin\theta_s}{\sqrt{1-\sin^2\theta_s}} + \frac{H\sin\theta_s}{\sqrt{\left(\frac{\beta}{\alpha}\right)^2 - \sin^2\theta_s}} + \frac{H_w\sin\theta_s}{\sqrt{\left(\frac{\beta}{\alpha_w}\right)^2 - \sin^2\theta_s}}.$$

It shows that θ_s must be less than the critical angle $\arcsin(\frac{\beta}{\alpha})$ since if $\theta_s = \arcsin(\frac{\beta}{\alpha})$, the offset X will be infinite. Physically, this is not possible. Figure 4 charts this behaviour for different S-wave velocities with a given P-wave velocity, water depth and reflector depth. It shows that the angle of incidence increases with offset but never exceeds the first critical angle. As a consequence, the incident SV-wave never changes its phase.

PHASE CHANGE OF P-SV CONVERTED WAVES CONVERTED AT MULTIPLE HORIZONTAL REFLECTORS

This analysis may readily be extended to a multilayered medium. Consider two isotropic, horizontal subsurface layers (Fig. 5). The horizontal slowness is constant along the raypath. Thus the take-off angle θ_{wp} at the source is related to the propagation angles through the sea-bed sediments and reflectors, θ_{1p}, θ_{2p}, θ_{2s} and the angle of incidence on the sea-bed receiver, θ_{1s}. This

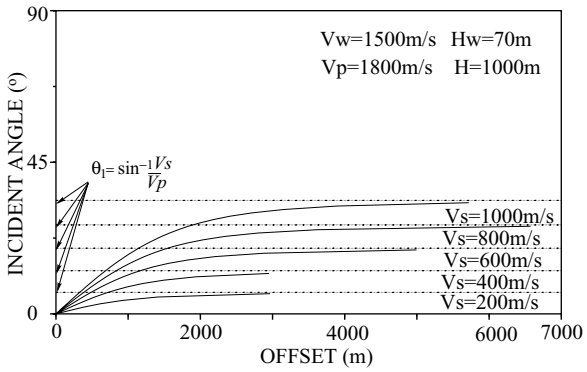

Figure 4 Angle of incidence versus offset for the case of a horizontal reflector. The straight lines are the critical angles corresponding to the S-wave velocities.

relationship is given by Snell's law,

$$\frac{\sin\theta_{\mathrm{wp}}}{\alpha_{\mathrm{w}}} = \frac{\sin\theta_{1\mathrm{p}}}{\alpha_1} = \frac{\sin\theta_{2\mathrm{p}}}{\alpha_2} = \frac{\sin\theta_{2\mathrm{s}}}{\beta_2} = \frac{\sin\theta_{1\mathrm{s}}}{\beta_1}.$$

Consequently, for any given offset the angle of incidence at the sensor is given by

$$\theta_{1\mathrm{s}} = \arcsin\left(\frac{\beta_1}{\alpha_{\mathrm{w}}}\sin\theta_{w}\right) = \arcsin\left(\frac{\beta_1}{\alpha_1}\sin\theta_{1\mathrm{p}}\right) = \arcsin\left(\frac{\beta_1}{\alpha_2}\sin\theta_{2\mathrm{p}}\right) = \arcsin\left(\frac{\beta_1}{\beta_2}\sin\theta_{2\mathrm{s}}\right).$$

Clearly, the maximum of $\theta_{1\mathrm{s}}$ is always smaller than the minimum of $\arcsin(\frac{\beta_1}{\beta_2})$, $\arcsin(\frac{\beta_1}{\alpha_2})$, $\arcsin(\frac{\beta_1}{\alpha_1})$ and $\arcsin(\frac{\beta_1}{\alpha_{\mathrm{w}}})$. If $\theta_{1\mathrm{s}}$ reached the maximum, the offset would be infinite. Whether the critical angle $\arcsin(\frac{\beta_1}{\alpha_1})$ is the smallest or not, $\theta_{1\mathrm{s}}$ is always less than it. The same result holds for the case of more than two reflectors. It thus appears that, provided the subsurface layers are laterally homogeneous, the inner critical angle will never be exceeded for the converted SV-waves, and no phase changes are therefore anticipated.

PHASE CHANGE OF P-SV CONVERTED WAVES CONVERTED AT A DIPPING REFLECTOR

The above conclusions must be modified if the reflector is dipping. This may be readily explained by a breakdown in the conservation of horizontal slowness due to the dipping layer. The dip may arise either at the target reflector or at the sea-bed. Figure 6 illustrates the case of a dipping reflector. In this case, Snell's law is written as

$$\frac{\sin\theta_{\mathrm{w}}}{\alpha_{\mathrm{w}}} = \frac{\sin\theta_{\mathrm{p}}}{\alpha} = \frac{\sin\theta_{\mathrm{s}}}{\beta}$$

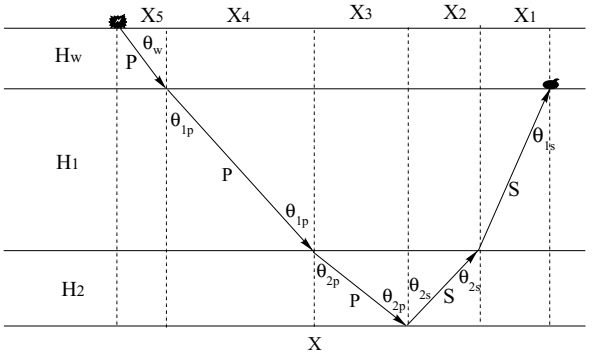

Figure 5 The P-SV converted wave raypath converted at two horizontal reflectors.

at the sea-bed and

$$\frac{\sin(\theta_s - \delta)}{\beta} = \frac{\sin(\theta_p + \delta)}{\alpha}$$

at the dipping reflector, where δ is the angle of dip. Rewriting this equation as

$$\theta_s = \delta + \arcsin\left[\frac{\beta}{\alpha}(\sin(\theta_p + \delta)\right],$$

the angle of incidence θ_s for the downdip raypath at the receiver always lies in the range

$$\delta \le \theta_s \le \delta + \arcsin\left(\frac{\beta}{\alpha}\right).$$

The relationship between the offset and the angle of incidence is

$$X = \frac{H}{1 + \tan\delta\tan\theta_s}\left[\tan\theta_s + \frac{\frac{\alpha}{\beta}\sin(\theta_s - \delta) - \tan\delta\sqrt{1 - \left[\frac{\alpha}{\beta}\sin(\theta_s - \delta)\right]^2}}{\sqrt{1 - \left[\frac{\alpha}{\beta}\sin(\theta_s - \delta)\right]^2} + \frac{\alpha}{\beta}\sin(\theta_s - \delta)\tan\delta}\right]$$

$$+\left[\frac{H_w\frac{\alpha_w}{\alpha}\left[\frac{\alpha}{\beta}\sin(\theta_s - \delta)\cos\delta - \sqrt{1 - \left[\frac{\alpha}{\beta}\sin(\theta_s - \delta)\right]^2}\sin\delta\right]}{\sqrt{1 - \left\{\frac{\alpha_w}{\alpha}\left[\frac{\alpha}{\beta}\sin(\theta_s - \delta)\cos\delta - \sqrt{1 - \left[\frac{\alpha}{\beta}\sin(\theta_s - \delta)\right]^2}\sin\delta\right]\right\}^2}}\right].$$

Thus, the angle of incidence can now exceed the critical angle at the water–sediment interface. For small values of β, this can occur for a relatively small subsurface dip. This point is illustrated in Figs 7 and 8, which show the variation of phase change with offset for a variety of target dips. This may be compared directly with Fig. 4. Note that the angle of dip imparts a maximum offset limit. The P-SV waves disappear if the offset exceeds this limit. It thus appears that a dip of only 5° is sufficient to move the incident SV-waves beyond the S-wave window. However, if the dip angle is negative in the case of an updipping reflector, e.g. in the opposite offset direction, θ_s is always less than the first critical angle, $\arcsin(\frac{\beta}{\alpha})$. Phase changes will not be expected. The phase change occurs only for one offset direction - hence the asymmetry.

Comparing Figs 7 and 8, we can see that the phase behaviours for SV-waves with various velocities at receivers are quite different especially for small angles of dip. For a lower SV-wave velocity (Fig. 7), the phase changes abruptly at near offsets corresponding to the phase change between the first and second critical angles. If the offset is larger than the offset corresponding to the second critical angle, the phase becomes stable with smooth variation. However, for a high SV-wave velocity (Fig. 8), the

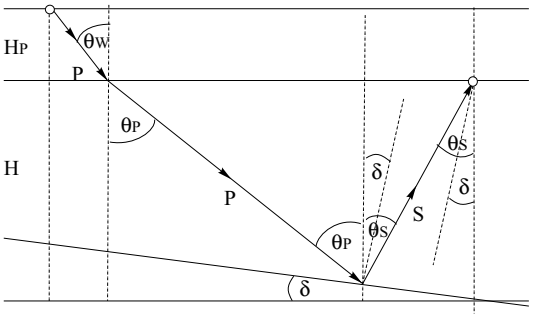

Figure 6 The P-SV wave raypath converted at a dipping reflector.

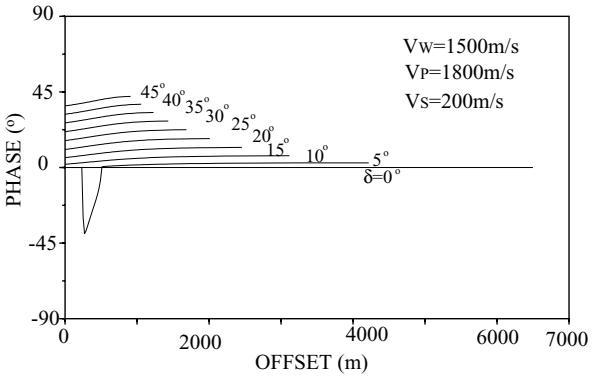

Figure 7 Phase change against offset for a target with angle of dip δ, with a low S-wave velocity. A water depth of 70 m and a target depth of 1000 m are used for the calculation.

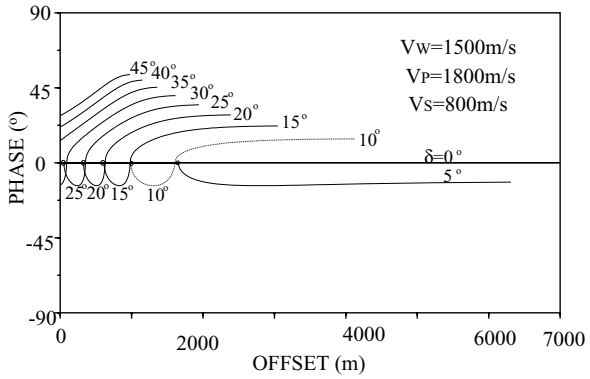

Figure 8 Phase change against offset for a target with angle of dip δ, with a high S-wave velocity. A water depth of 70 m and a target depth of 1000 m are used for the calculation.

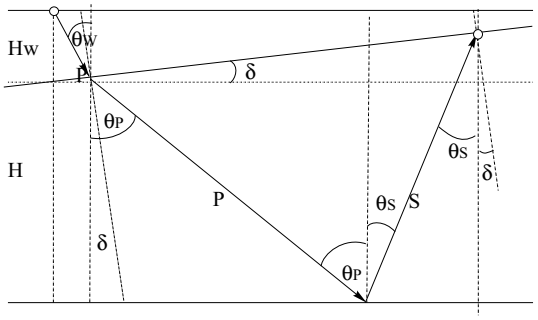

Figure 9 The P-SV wave raypath recorded at a dipping sea-bed.

phase does not change at near offsets corresponding to the first critical angle. If the offset exceeds the offset corresponding to the first critical angle, the phase gradually decreases and then increases. The phase is more stable for the low S-velocity than for the high S-wave velocity.

PHASE CHANGE OF P-SV CONVERTED WAVES RECORDED AT A DIPPING SEA-BED

Here the case of a dipping sea-bed is discussed. In this case, the conservation of horizontal slowness does not break down, but an extra angle must be added to the angle of incidence of the S-wave recorded at the sea-bed. Figure 9 illustrates this point. In

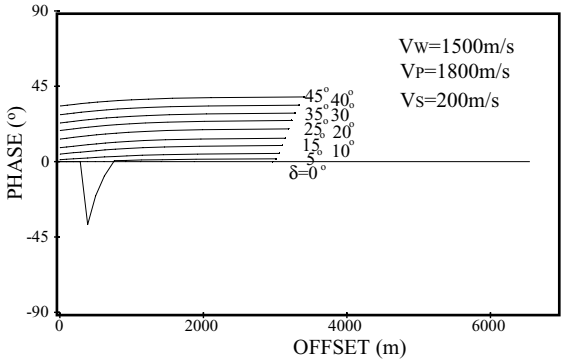

Figure 10 Phase change against offset for a dipping sea-bed with angle of dip δ, with a low S-wave velocity. A water depth of 70 m and a target depth of 1000 m are used for the calculation.

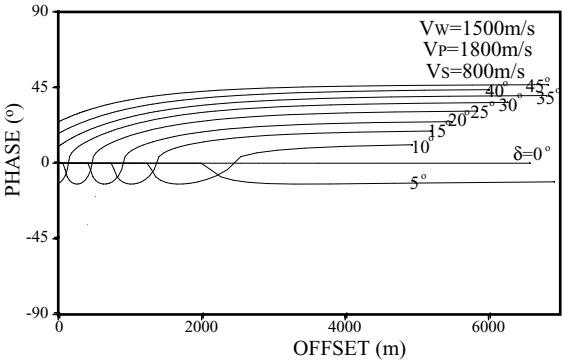

Figure 11 Phase change against offset for a dipping sea-bed with angle of dip δ, with a high S-wave velocity. A water depth of 70 m and a target depth of 1000 m are used for the calculation.

this case, at the reflector, Snell's law can be written as

$$\frac{\sin(\theta_s)}{\beta} = \frac{\sin(\theta_p)}{\alpha}$$

and at the dipping sea-bed it can be written as

$$\frac{\sin(\theta_{ww})}{\alpha_w} = \frac{\sin(\theta_{pw})}{\alpha} = \frac{\sin(\theta_s + \delta)}{\beta}.$$

Note that the angle of incidence at the dipping sea-bed is $\theta_s + \delta$, not θ_s. θ_s is the angle of incidence of an S-wave at the horizontal reflector. The first critical angle of phase change at the dipping sea-bed is $\arcsin(\frac{\beta}{\alpha})$. Note that the maximum θ_s at the reflector is also $\arcsin(\frac{\beta}{\alpha})$. The angle of incidence at the sea-bed, $\theta_s + \delta$, can exceed this critical angle and the phase change should occur. If δ is less than zero, $\theta_s + \delta$ can never reach the critical angle. This shows an asymmetric change in phase for the dipping sea-bed. The offset at which the phase changes depends on the angle of dip δ. The relationship between the offset and the angles of incidence is

$$X = \frac{H(\tan\theta_p + \tan\theta_s)}{1 - \tan\delta\tan\theta_s} + \frac{H_w \tan\theta_w(1 + \tan\delta\tan\theta_p)}{1 + \tan\delta\tan\theta_w}.$$

Figures 10 and 11 show this relationship for different V_s. Comparing Figs 10 and 11 with Figs 7 and 8, we can see that the phase behaviour caused by a dipping sea-bed is similar to that caused by a dipping reflector.

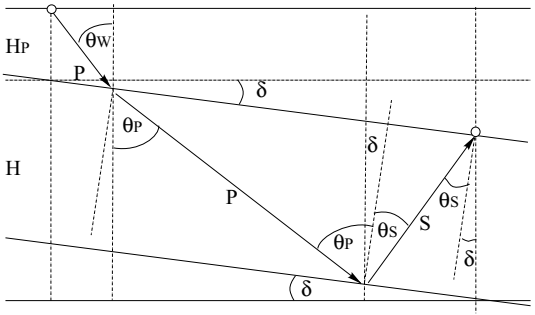

Figure 12 The P-SV wave raypath recorded at a dipping sea-bed and converted at a dipping reflector. The dipping sea-bed and reflector are parallel.

PHASE CHANGE OF P-SV CONVERTED WAVES RECORDED AT A DIPPING SEA-BED AND CONVERTED AT A DIPPING REFLECTOR

Firstly, a simple case in which the dipping sea-bed is parallel to the dipping reflector is discussed. Figure 12 illustrates this point. In this case, θ_s never exceeds the first critical angle, $\arcsin(\frac{\beta}{\alpha})$. We cannot expect a phase change. In fact, the phase change is caused by the non-parallel geometry setting between the dipping reflector and the dipping sea-bed. In the case of a non-parallel dipping reflector and sea-bed, we can rotate the geometry setting so that either the reflector or the sea-bed is horizontal. If the rotated sea-bed is horizontal, the case is similar to the dipping reflector. If the rotated reflector is horizontal, the case is similar to the dipping sea-bed. Both cases are discussed in the above sections.

PLANE BODY WAVES INCIDENT ON AN INTERFACE BETWEEN WATER AND A WEAKLY TIV MEDIUM

For a TIV medium, every vertical plane is a plane of symmetry. The P- and S-wave polarizations lying parallel to this plane are labelled qP and qSV for ease of use. Both qP and qSV are decoupled from the pure SH-wave which has a polarization normal to the symmetry plane. The behaviour of the plane wave recorded at this interface is like that at the interface between the water and an isotropic medium. The analysis in the Appendix can easily be extended to the anisotropy case by replacing the velocities of the P- and S-waves with the velocities of the qP- and qSV-waves. For the incident qP-wave, there is no phase change. For the incident qSV-wave, there are two critical angles at which a phase change occurs. The first critical angle is at $\frac{\beta_v(\theta)}{\alpha(\theta)} = \sin\theta$ and the second critical angle is at $\frac{\alpha_w(\theta)}{\alpha(\theta)} = \sin\theta$. Here θ is the phase angle between the wavefront normal and the vertical axis. The velocities of a TIV medium can be approximately written as (Thomsen 1986)

$$\alpha^2(\theta) = \alpha_0^2[1 + \varepsilon \sin^2\theta + D^*(\theta)],$$

$$\beta_v^2(\theta) = \beta_0^2\left[1 + \left(\frac{\alpha_0}{\beta_0}\right)^2 \varepsilon \sin^2\theta - \left(\frac{\alpha_0}{\beta_0}\right)^2 D^*(\theta)\right],$$

$$\beta_h^2(\theta) = \beta_0^2[1 + 2\gamma \sin^2\theta],$$

$$D^*(\theta) = \frac{1}{2}\left[1 - \left(\frac{\beta_0}{\alpha_0}\right)^2\right]\left[\sqrt{1 + \frac{4\delta^*}{\left[1 - \left(\frac{\beta_0}{\alpha_0}\right)^2\right]^2}\sin^2\theta\cos_2\theta + \frac{4\left[1 - \left(\frac{\beta_0}{\alpha_0}\right)^2 + \varepsilon\right]\varepsilon}{\left[1 - \left(\frac{\beta_0}{\alpha_0}\right)^2\right]^2}\sin^4\theta} - 1\right],$$

where ε, γ and δ^* are the Thomsen parameters which define the anisotropy of the TIV medium. Figure 9 shows the P-SV wave raypath in the anisotropic medium. Note that the direction of the raypath is defined by the group angle ϕ, not the phase angle.

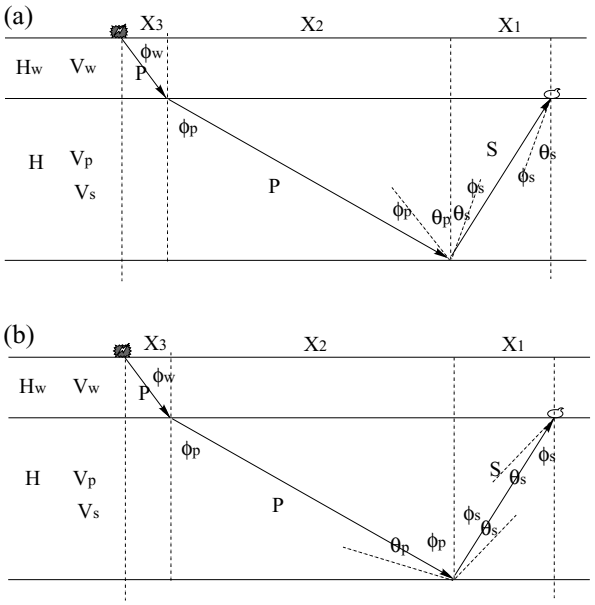

Figure 13 The P-SV wave raypath converted at a horizontal reflector in an anisotropic medium.

The relationship between the phase angle and the group angle can be written as (Thomsen 1986)

$$\tan\phi = \frac{\tan\theta + \dfrac{1}{\nu}\dfrac{\mathrm{d}\nu}{\mathrm{d}\theta}}{1 - \dfrac{\tan\theta}{\nu}\dfrac{\mathrm{d}\nu}{\mathrm{d}\theta}} = \tan(\theta + \xi)$$

or

$$\phi = \theta + \xi,$$

where $\tan\xi = \frac{1}{\nu}\frac{\mathrm{d}\nu}{\mathrm{d}\theta}$ and ν is the velocity, α, β_{v} or b_{h}. Note that Snell's law is applied only to the phase angle. The maximum phase angle of the S-wave at the reflector is the solution of $\frac{\beta_{\mathrm{v}}(\theta)}{\alpha(\theta)} = \sin\theta$, which is the first critical angle. Regardless of whether the corresponding group angle is larger or smaller than the phase angle, only the raypath for which the phase angle is less than the first critical angle exists. Figure 13 shows two cases. The first case occurs when the phase angle is greater than the group angle (Fig. 13a). The second case occurs when the group angle is greater than the phase angle (Fig. 13b). In both cases, the phase angle of the qSV-wave leg cannot exceed the first critical angle. This means the incident qSV-wave at the sea-bed never changes its phase. This analysis shows that anisotropy does not affect the phase character of the P-SV converted wave. The phase change is caused only by the non-parallel relationship between the dipping sea-bed and the dipping reflector.

DATA EXAMPLES

To investigate the phase change of P-SV converted waves, two sets of field data are analysed. These data are derived from the Valhall field (Thomsen *et al*. 1997) and a field in the central North Sea. Figure 14 shows a part of the image of the converted wave of the Valhall field. This image shows that the reflectors under the Valhall field and the sea-bed are horizontal, so that we cannot expect phase change from the P-SV converted wave. Here some examples from the Valhall field are shown. Because this phenomenon is more affected by the S-wave velocity at the receiver than at the deep reflector, the common-receiver gathers are selected so as to focus on this receiver-consistent phenomenon. For each gather, one event around 1.5 s is selected and the wavelet phase estimated as follows:

1 Preprocess to eliminate guided waves and other linear events mute and then apply a band-pass filter.

2 Apply an anisotropic moveout correction to flatten the P-SV converted waves on the radial component.

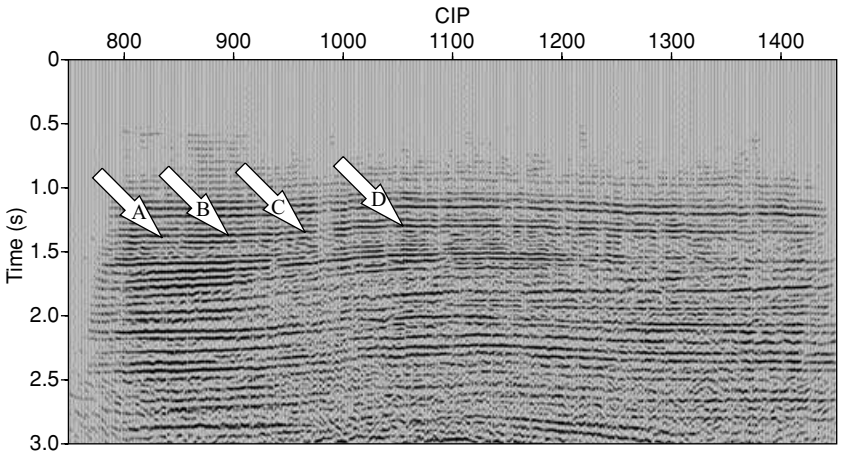

Figure 14 The shallow part of the image of the Valhall field. The white arrows indicate the examples shown on Fig. 15.

3 Select the desired time window around the chosen event thus obtaining $s(t)$.
4 Calculate the Hilbert transform of this signal: $h(t)$.
5 Calculate the average of the instantaneous phase function $\arctan(\frac{h(t)}{s(t)})$ around the maximum of the analytic envelope formed by $A(t) = \sqrt{s^2(t) + h^2(t)}$.

This method was used to analyse the Valhall field data. Figure 15 shows some examples of the data and the corresponding phase values for the selected events. Inspection of the resulting estimates reveals that only little or no systematic phase change with offset occurs. This coincides with the theoretical analysis for a horizontal reflector and sea-bed. The same method has also been applied to another field data set in the central North Sea for which the results show a phase change in the negative offset (Fig. 16). Unfortunately, it is not possible to show the seismic data for this survey, but this behaviour could be related to a dipping reflector or dipping sea-bed.

The data analysis shows that the phase behaviour of the P-SV converted wave falls into two broad categories of effects that coincide with the theoretical analysis. The predominant effect belongs to category A (Fig. 15), for which there is little or no phase change with offset. Category B effects (Fig. 16) occur occasionally, and are distinguished by a phase change in either the positive or negative offset direction, but not both.

CONCLUSIONS

The phase characteristics of P-SV converted waves have been analysed. The phase changes when the angle of incidence of the SV-wave exceeds the critical angle of the S-wave window at the sea-bed. However, considering the reality of the P-SV wave raypath, this phase change may not occur. Theoretical analysis for several cases shows that the phase change does not occur when both reflector and sea-bed sediment are horizontal. Either a dipping reflector or a dipping sea-bed can cause the phase change. However, if the dipping sea-bed is parallel to the reflector, the phase change does not occur. The phase change occurs only when the reflector and sea-bed are not parallel. In this case, the phase change is asymmetric with the offset direction. Analysing the TIV medium shows that the anisotropy does not cause the phase change.

The analysis of phase estimates from OBC data suggests that two categories of effects may arise in practice. Category A occurs most often, and may readily be explained by a horizontally layered medium. This finding highlights the robustness of the converted wave for imaging purposes. Category B exhibits more subtle effects, which may arise only infrequently. These effects distinguish P-SV converted waves in a marine setting from the behaviour of the directly generated S-waves on land, for which the acquisition geometry alone dictates that the shear-wave window must be exceeded at large offsets.

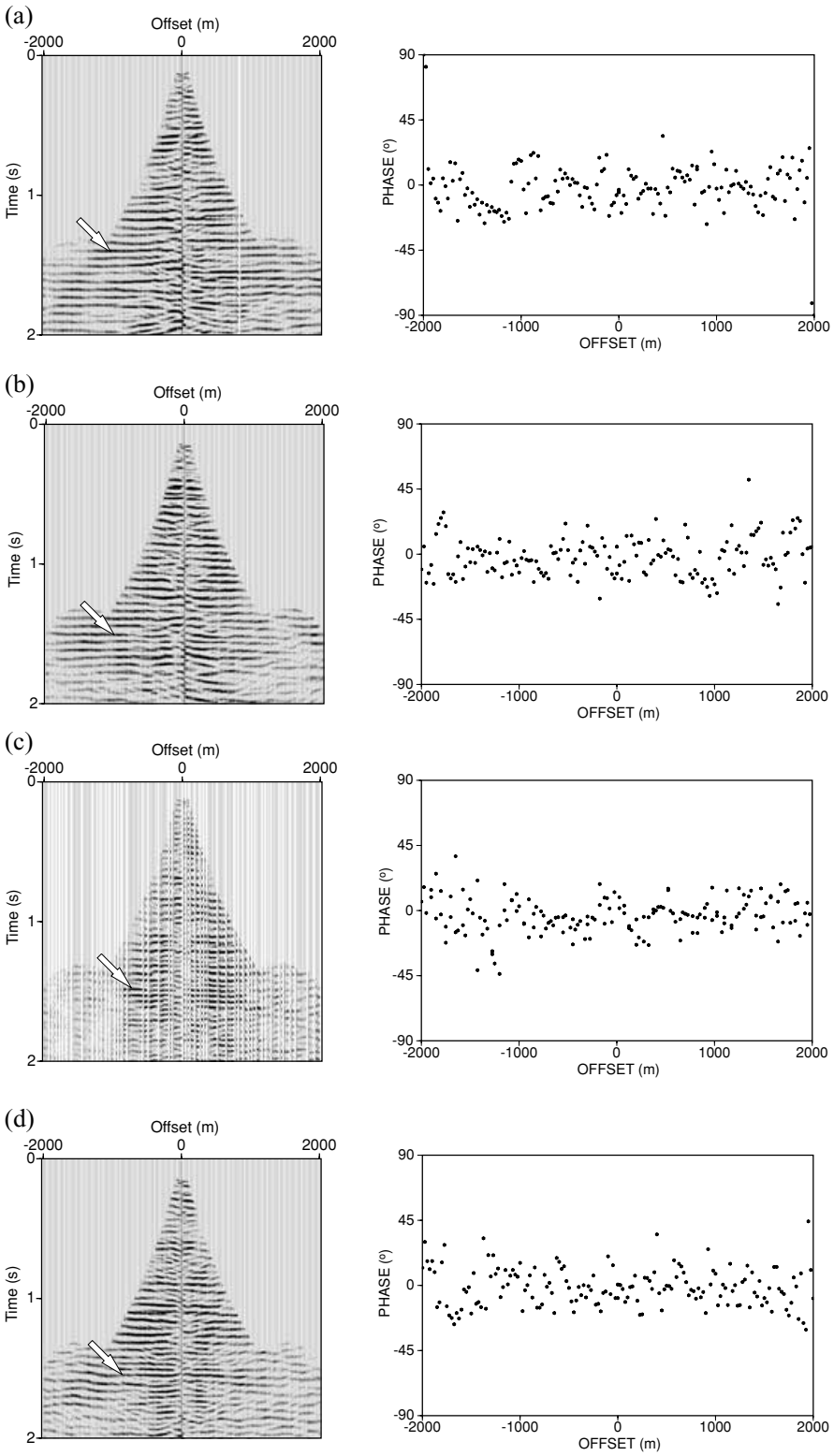

Figure 15 The common-receiver gathers and the corresponding phase change for the events indicated by the arrows on the common-receiver gathers. (a), (b), (c), (d) correspond to the arrows A, B, C, D, respectively, in Fig. 14.

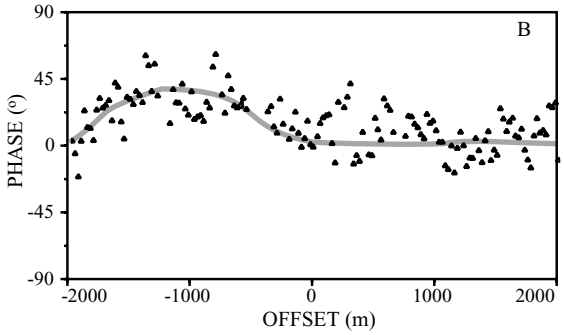

Figure 16 Phase estimates showing an asymmetric phase change with offset for the data from a field in the central North Sea.

ACKNOWLEDGEMENTS

The author thanks Professor Colin MacBeth of Heriot-Watt University for initiating this study and giving valuable suggestions and advice for writing the manuscript, and Dr Xiang-Yang Li for useful discussions. The author also thanks BP-Amoco and the Valhall licence partners for permission to show the Valhall data. This work is funded by the Edinburgh Anisotropy Project of the British Geological Survey and is published with the permission of the Executive Director of the British Geological Survey (NERC), and the sponsors of the Edinburgh Anisotropy Project.

REFERENCES

Aki K.T. and Richards P.G. 1980. *Quantitative Seismology: Theory and Methods*, **Vol. 1.** W.H. Freeman.

Berg E., Svenning B. and Martin J. 1994. SUMIC – a new strategic tool for exploration and reservoir mapping. 56th EAGE Meeting, Vienna, Austria, Extended Abstracts, G055.

Booth D. and Crampin S. 1985. Shear-wave polarization on a curved wave front at an isotropic free-surface. *Geophysical Journal of the Royal Astronomical Society* **83,** 31–45.

Brekhovskikh L.M. 1980. *Waves in Layered Media*. Academic Press, Inc.

Dai H.-C., Li X.-Y. and Mueller M. 2000. The effects of gas clouds on converted-wave imaging: a case study from Valhall. 62nd EAGE Conference, Glasgow, UK, Extended Abstracts, P0103.

Evans R. 1984. Effects of the free surface on shear wave trains. *Geophysical Journal of the Royal Astronomical Society* **7,** 165–172.

Li X.-Y., Kuhnel T. and MacBeth C. 1996. Mixed mode AVO response in fractured media. 66th SEG Meeting, Denver, Colorado, USA, Expanded Abstracts, 1822–1825.

MacBeth C. 1997. *Three-Component Recording Distortion at a Water–Sediment Interface*. Annual Report of the Edinburgh Anisotropy Project 4.

MacBeth C. 1998. An essential processing correction for sea-bed recording. 60th EAGE Conference, Leipzig, Germany, Extended Abstracts, 2–06.

Mazzotti A. 1991. Amplitude, phase and frequency versus offset application. *Geophysical Prospecting* **39,** 863–886.

Nuttli O. 1961. The effect of the earth's surface on the S-wave particle motion. *Bulletin of the Seismological Society of America* **58,** 237–246.

Thomsen L. 1986. Weak elastic anisotropy. *Geophysics* **51,** 1954–1966.

Thomsen L., Barkved O., Haggard B., Kommedal J. and Rosland B. 1997. Converted wave imaging of Valhall Reservoir. 59th EAGE Conference, Geneva, Switzerland, Extended Abstracts, B048.

APPENDIX

Velocity field recorded at the interface between water and an isotropic solid

The problem of a plane body wave incident upon a fluid interface has been solved in previous work for the isotropic case (e.g. Aki and Richards 1980; Brekhovskikh 1980), but MacBeth (1997) re-derived these results to aid physical understanding. Consider wave propagation confined to a vertical x–z plane, with polarization lying in this plane. The total velocity field at the interface

for an incident P-wave can be written as (MacBeth 1997)

$$v_x^{\mathrm{p}}(0) = \frac{2\alpha s_x s_{\mathrm{zp}}(\rho_{\mathrm{w}} + 2\rho\beta^2 s_{\mathrm{zw}} s_{\mathrm{zs}})}{\rho s_{\mathrm{zw}} + \rho_{\mathrm{w}} s_{\mathrm{zp}} - 4\rho\beta^2 s_x^2 s_{\mathrm{zw}}(1 - \beta^2 s_x^2 - \beta^2 s_{\mathrm{zs}} s_{\mathrm{zp}})} \mathrm{e}^{\mathrm{i}\omega s_x x}$$

and

$$v_z^{\mathrm{p}}(0) = \frac{2\rho\alpha s_{\mathrm{zw}} s_{\mathrm{zp}}(1 - 2\beta^2 s_x^2)}{\rho s_{\mathrm{zw}} + \rho_w s_{\mathrm{zp}} - 4\rho\beta^2 s_x^2 s_{\mathrm{zw}}(1 - \beta^2 s_x^2 - \beta^2 s_{\mathrm{zs}} s_{\mathrm{zp}})} \mathrm{e}^{\mathrm{i}\omega s_x x},$$

where the horizontal slowness is s_x and the vertical slownesses are $s_{\mathrm{zp}} = \sqrt{\alpha^{-2} - s_x^2}$, $s_{\mathrm{zs}} = \sqrt{\beta^{-2} - s_x^2}$ and $s_{\mathrm{zw}} = \sqrt{\alpha_{\mathrm{w}}^{-2} - s_x^2}$, with each polarization vector being of unit magnitude. The P- and S-wave velocities of the sediment media and the P-wave velocity of the water are given by α, β and α_{w}, respectively, and ρ and ρ_{w} are the densities of sediment media and water.

The total velocity field at the interface for an incident SV-wave can be written as (MacBeth 1997)

$$v_x^{\mathrm{s}}(0) = \frac{2\beta s_{\mathrm{zs}}(\rho_{\mathrm{w}} s_{\mathrm{zp}} + \rho s_{\mathrm{zw}} - 2\rho\beta^2 s_x^2 s_{\mathrm{zw}})}{\rho s_{\mathrm{zw}} + \rho_{\mathrm{w}} s_{\mathrm{zp}} - 4\rho\beta^2 s_x^2 s_{\mathrm{zw}}(1 - \beta^2 s_x^2 - \beta^2 s_{\mathrm{zs}} s_{\mathrm{zp}})} \mathrm{e}^{\mathrm{i}\omega s_x x}$$

and

$$v_z^{\mathrm{s}}(0) = \frac{-4\rho\beta^3 s_x s_{\mathrm{zp}} s_{\mathrm{zs}} s_{\mathrm{zw}}}{\rho s_{\mathrm{zw}} + \rho_{\mathrm{w}} s_{\mathrm{zp}} - 4\rho\beta^2 s_x^2 s_{\mathrm{zw}}(1 - \beta^2 s_x^2 - \beta^2 s_{\mathrm{zs}} s_{\mathrm{zp}})} \mathrm{e}^{\mathrm{i}\omega s_x x}.$$

For the incident SH-wave, the water–solid interface acts as a free surface, so the reflected wave is of the same type, amplitude and phase. The waves suffer no conversion upon reflection, and the free surface is a perfect reflector. Thus the amplitude of the motion at the boundary is the sum of incident and reflected waves, that is, twice the amplitude of the incident wave.

The total velocity fields can also be written as a function of angle of incidence. For an incident P-wave with angle of incidence angle θ we have

$$s_x = \frac{\sin\theta}{\alpha},$$

$$s_{\mathrm{zs}} = \sqrt{\left(\frac{1}{\beta}\right)^2 - \left(\frac{\sin\theta}{\alpha}\right)^2},$$

$$s_{\mathrm{zp}} = \sqrt{\left(\frac{1}{\alpha}\right)^2 - \left(\frac{\sin\theta}{\alpha}\right)^2} = \frac{\cos\theta}{\alpha}$$

and

$$s_{\mathrm{zw}} = \sqrt{\left(\frac{1}{\alpha_{\mathrm{w}}}\right)^2 - \left(\frac{\sin\theta}{\alpha}\right)^2}.$$

Substituting, we have (at $x = 0$)

$$v_x^{\mathrm{p}}(0) = \frac{\sin 2\theta \left[\dfrac{\rho_{\mathrm{w}}}{\rho} + 2\left(\dfrac{\beta}{\alpha}\right)^2 \sqrt{\left(\dfrac{\alpha}{\beta}\right)^2 - \sin^2\theta} \sqrt{\left(\dfrac{\alpha}{\alpha_{\mathrm{w}}}\right)^2 - \sin^2\theta}\right]}{\left[\left[1 - \left(\dfrac{2\beta\sin\theta}{\alpha}\right)^2\right] \sqrt{\left(\dfrac{\alpha}{\alpha_{\mathrm{w}}}\right)^2 - \sin^2\theta} + \dfrac{\rho_{\mathrm{w}}}{\rho}\cos\theta + \left(\dfrac{2\beta}{\alpha}\sin\theta\right)^2 \sqrt{\left(\dfrac{\alpha}{\alpha_{\mathrm{w}}}\right)^2 - \sin^2\theta} \left[\sin^2\theta + \cos\theta \sqrt{\left(\dfrac{\alpha}{\beta}\right)^2 - \sin^2\theta}\right]\right]} = A_x(\theta)\mathrm{e}^{\mathrm{i}\phi_x(\theta)}$$

and

$$v_z^{\mathrm{p}}(0) = \frac{2\cos\theta\sqrt{\left(\frac{\alpha}{\alpha_{\mathrm{w}}}\right)^2 - \sin^2\theta}\left[1 - 2\left(\frac{\beta\sin\theta}{\alpha}\right)^2\right]}{\left[\left[1 - \left(\frac{2\beta\sin\theta}{\alpha}\right)^2\right]\sqrt{\left(\frac{\alpha}{\alpha_{\mathrm{w}}}\right)^2 - \sin^2\theta} + \frac{\rho_{\mathrm{w}}}{\rho}\cos\theta \right.} \\ \left. + \left(\frac{2\beta}{\alpha}\sin\theta\right)^2\sqrt{\left(\frac{\alpha}{\alpha_{\mathrm{w}}}\right)^2 - \sin^2\theta}\left[\sin^2\theta + \cos\theta\sqrt{\left(\frac{\alpha}{\beta}\right)^2 - \sin^2\theta}\right]\right] = A_z(\theta)\mathrm{e}^{\mathrm{i}\phi_z(\theta)}.$$

The velocity fields are complex functions if the square roots are imaginary numbers. In that case, they decompose into the amplitude functions $A_x(\theta)$ or $A_z(\theta)$ and the phase functions $\mathrm{e}^{\mathrm{i}\phi_x(\theta)}$ or $\mathrm{e}^{\mathrm{i}\phi_x(\theta)}$. For the P-wave, because $\frac{\alpha}{\beta} > 1$ and $\frac{\alpha}{\alpha_{\mathrm{w}}} > 1$, all the square roots are real and $\phi_x = \phi_z = 0$. There is no phase change at all. For an incident SV-wave,

$$s_x = \frac{\sin\theta}{\beta},$$

$$s_{zs} = \sqrt{\left(\frac{1}{\beta}\right)^2 - \left(\frac{\sin\theta}{\beta}\right)^2} = \frac{\cos\theta}{\beta},$$

$$s_{\mathrm{zp}} = \sqrt{\left(\frac{1}{\alpha}\right)^2 - \left(\frac{\sin\theta}{\beta}\right)^2}$$

and

$$s_{\mathrm{zw}} = \sqrt{\left(\frac{1}{\alpha_{\mathrm{w}}}\right)^2 - \left(\frac{\sin\theta}{\beta}\right)^2}.$$

We have (at $x = 0$)

$$v_x^s(0) = \frac{2\cos\theta\left[\cos 2\theta\sqrt{\left(\frac{\beta}{\alpha_{\mathrm{w}}}\right)^2 - \sin^2\theta} + \frac{\rho_{\mathrm{w}}}{\rho}\sqrt{\left(\frac{\beta}{\alpha}\right)^2 - \sin^2\theta}\right]}{\left[\cos^2 2\theta\sqrt{\left(\frac{\beta}{\alpha_{\mathrm{w}}}\right)^2 - \sin^2\theta} + \frac{\rho_{\mathrm{w}}}{\rho}\sqrt{\left(\frac{\beta}{\alpha}\right)^2 - \sin^2\theta} \right.} \\ \left. + 4\sin^2\theta\cos\theta\sqrt{\left(\frac{\beta}{\alpha_{\mathrm{w}}}\right)^2 - \sin^2\theta}\sqrt{\left(\frac{\beta}{\alpha}\right)^2 - \sin^2\theta}\right] = B_x(\theta)\mathrm{e}^{\mathrm{i}\phi_x(\theta)}$$

and

$$v_z^s(0) = \frac{\left[-4\sin\theta\cos\theta\sqrt{\left(\frac{\beta}{\alpha}\right)^2 - \sin^2\theta}\sqrt{\left(\frac{\beta}{\alpha_{\mathrm{w}}}\right)^2 - \sin^2\theta}\right]}{\left[\cos^2 2\theta\sqrt{\left(\frac{\beta}{\alpha_{\mathrm{w}}}\right)^2 - \sin^2\theta} + \frac{\rho_{\mathrm{w}}}{\rho}\sqrt{\left(\frac{\beta}{\alpha}\right)^2 - \sin^2\theta} \right.} \\ \left. + 4\sin^2\theta\cos\theta\sqrt{\left(\frac{\beta}{\alpha_{\mathrm{w}}}\right)^2 - \sin^2\theta}\sqrt{\left(\frac{\beta}{\alpha}\right)^2 - \sin^2\theta}\right] = B_z(\theta)\mathrm{e}^{\mathrm{i}\phi_z(\theta)}.$$

If $\theta \le \theta_1 = \arcsin(\frac{\beta}{\alpha})$, then

$$v_x^s(0) = \frac{2\cos\theta\left[\cos 2\theta\sqrt{\left(\frac{\beta}{\alpha_w}\right)^2 - \sin^2\theta} + \frac{\rho_w}{\rho}\sqrt{\left(\frac{\beta}{\alpha}\right)^2 - \sin^2\theta}\right]}{\left[\begin{array}{l}\cos^2 2\theta\sqrt{\left(\frac{\beta}{\alpha_w}\right)^2 - \sin^2\theta} + \frac{\rho_w}{\rho}\sqrt{\left(\frac{\beta}{\alpha}\right)^2 - \sin^2\theta} \\ \quad +4\sin^2\theta\cos\theta\sqrt{\left(\frac{\beta}{\alpha_w}\right)^2 - \sin^2\theta}\sqrt{\left(\frac{\beta}{\alpha}\right)^2 - \sin^2\theta}\end{array}\right]} = B_x(\theta)e^{i\phi_x(\theta)}$$

and

$$v_z^s(0) = \frac{-4\sin\theta\cos\theta\sqrt{\left(\frac{\beta}{\alpha}\right)^2 - \sin^2\theta}\sqrt{\left(\frac{\beta}{\alpha_w}\right)^2 - \sin^2\theta}}{\left[\begin{array}{l}\cos^2 2\theta\sqrt{\left(\frac{\beta}{\alpha_w}\right)^2 - \sin^2\theta} + \frac{\rho_w}{\rho}\sqrt{\left(\frac{\beta}{\alpha}\right)^2 - \sin^2\theta} \\ \quad +4\sin^2\theta\cos\theta\sqrt{\left(\frac{\beta}{\alpha_w}\right)^2 - \sin^2\theta}\sqrt{\left(\frac{\beta}{\alpha}\right)^2 - \sin^2\theta}\end{array}\right]} = B_z(\theta)e^{i\phi_z(\theta)}.$$

Because all the square roots are real, $\phi_x = \phi_z = 0$. If $\theta_1 = \arcsin(\frac{\beta}{\alpha}) \le \theta \le \theta_2 = \arcsin(\frac{\beta}{\alpha_w})$, then

$$v_x^s(0) = \frac{2\cos\theta\left[\frac{\rho_w}{\rho}\sqrt{\sin^2\theta - \left(\frac{\beta}{\alpha}\right)^2} - i\cos 2\theta\sqrt{\left(\frac{\beta}{\alpha_w}\right)^2 - \sin^2\theta}\right]}{\left[\begin{array}{l}\left[\frac{\rho_w}{\rho} + 4\sin^2\theta\cos\theta\sqrt{\left(\frac{\beta}{\alpha_w}\right)^2 - \sin^2\theta}\right]\sqrt{\sin^2\theta - \left(\frac{\beta}{\alpha}\right)^2} \\ \quad -i\cos^2 2\theta\sqrt{\left(\frac{\beta}{\alpha_w}\right)^2 - \sin^2\theta}\end{array}\right]} = B_x(\theta)e^{i(\phi-\varphi)}$$

and

$$v_z^s(0) = \frac{-4\sin\theta\cos\theta\sqrt{\sin^2\theta - \left(\frac{\beta}{\alpha}\right)^2}\sqrt{\left(\frac{\beta}{\alpha_w}\right)^2 - \sin^2\theta}}{\left[\begin{array}{l}\left[\frac{\rho_w}{\rho} + 4\sin^2\theta\cos\theta\sqrt{\left(\frac{\beta}{\alpha_w}\right)^2 - \sin^2\theta}\right]\sqrt{\sin^2\theta - \left(\frac{\beta}{\alpha}\right)^2} \\ \quad -i\cos^2 2\theta\sqrt{\left(\frac{\beta}{\alpha_w}\right)^2 - \sin^2\theta}\end{array}\right]} = B_z(\theta)e^{i\phi},$$

where $\phi_x = \phi - \varphi$, $\phi_z = \phi$ and

$$\phi = \arctan\frac{\cos^2 2\theta\sqrt{\left(\frac{\beta}{\alpha_w}\right)^2 - \sin^2\theta}}{\sqrt{\sin^2\theta - \left(\frac{\beta}{\alpha}\right)^2}\left[\frac{\rho_w}{\rho} + 4\sin^2\theta\cos\theta\sqrt{\left(\frac{\beta}{\alpha_w}\right)^2 - \sin^2\theta}\right]}$$

and

$$\varphi = \arctan \frac{\cos^2 2\theta \sqrt{\left(\frac{\beta}{\alpha_w}\right)^2 - \sin^2\theta}}{\frac{\rho_w}{\rho}\sqrt{\sin^2\theta - \left(\frac{\beta}{\alpha}\right)^2}}.$$

If $\theta_1 = \arcsin(\frac{\beta}{\alpha}) \le \theta_2 = \arcsin(\frac{\beta}{\alpha_w}) \le \theta$, then

$$v_x^s(0) = \frac{2\cos\theta\left[\cos 2\theta\sqrt{\sin^2\theta - \left(\frac{\beta}{\alpha_w}\right)^2} + \frac{\rho_w}{\rho}\sqrt{\sin^2\theta - \left(\frac{\beta}{\alpha}\right)^2}\right]}{\left[\left[\cos^2 2\theta\sqrt{\sin^2\theta - \left(\frac{\beta}{\alpha_w}\right)^2} + \frac{\rho_w}{\rho}\sqrt{\sin^2\theta - \left(\frac{\beta}{\alpha}\right)^2}\right] - \mathrm{i}\left[4\sin^2\theta\cos\theta\sqrt{\sin^2\theta - \left(\frac{\beta}{\alpha_w}\right)^2}\sqrt{\sin^2\theta - \left(\frac{\beta}{\alpha}\right)^2}\right]\right]} = B_x(\theta)\mathrm{e}^{\mathrm{i}\phi}$$

and

$$v_z^s(0) = \frac{-\mathrm{i}4\sin\theta\cos\theta\sqrt{\sin^2\theta - \left(\frac{\beta}{\alpha}\right)^2}\sqrt{\sin^2\theta - \left(\frac{\beta}{\alpha_w}\right)^2}}{\left[\left[\cos^2 2\theta\sqrt{\sin^2\theta - \left(\frac{\beta}{\alpha_w}\right)^2} + \frac{\rho_w}{\rho}\sqrt{\sin^2\theta - \left(\frac{\beta}{\alpha}\right)^2}\right] - \mathrm{i}\left[4\sin^2\theta\cos\theta\sqrt{\sin^2\theta - \left(\frac{\beta}{\alpha_w}\right)^2}\sqrt{\sin^2\theta - \left(\frac{\beta}{\alpha}\right)^2}\right]\right]} = A_z(\theta)\mathrm{e}^{\mathrm{i}(\phi - \frac{\pi}{2})},$$

where $\phi_x = \phi - \varphi$, $\phi_z = \phi - \frac{\pi}{2}$ and

$$\phi = \arctan \frac{2\sin 2\theta \sin\theta\sqrt{\sin^2\theta - \left(\frac{\beta}{\alpha_w}\right)^2}\sqrt{\sin^2\theta - \left(\frac{\beta}{\alpha}\right)^2}}{\cos^2 2\theta\sqrt{\sin^2\theta - \left(\frac{\beta}{\alpha_w}\right)^2} + \frac{\rho_w}{\rho}\sqrt{\sin^2\theta - \left(\frac{\beta}{\alpha}\right)^2}}.$$

From the above discussion, we know that for an incident P-wave, there is no phase change. However, for an incident SV-wave, when the angle of incidence exceeds the critical angle, there is a phase change.